An observational test of the origin of accelerating moment release before large earthquakes

A. Mignan,[1] D. D. Bowman,[2] and G. C. P. King[1]

Received 2 March 2006; revised 19 June 2006; accepted 2 August 2006; published 11 November 2006.

[1] A progressive increase of seismic activity distributed over a wide region around a future earthquake epicenter is termed accelerating moment release (AMR). This phenomenon has been observed in several studies over the last 15 years, although there is no consensus about the physical origin of the effect. In a recent hypothesis known as the stress accumulation (SA) model, the AMR is thought to result from the last stage of loading in the earthquake cycle. In this view, the increasing seismicity is due to minor stress release as the whole region becomes sufficiently stressed for the major event to occur. The stress accumulation model makes specific predictions about the distribution of events in an AMR sequence. Because the AMR is predicted to be a result of loading on the main fault, the precursory activity should be concentrated in the positive lobes of the far-field stresses calculated by a backslip dislocation model of the main shock. To test this model, AMR is first found in optimal circular regions around the epicenters of each of the $M_w \geq 6.5$ earthquakes in central and southern California since 1950. A backslip dislocation model is then used to determine which of the precursory events occur in the regions predicted by stress accumulation. AMR is shown to occur preferentially in the lobes of the backslip stress field predicted by the stress accumulation model.

Citation: Mignan, A., D. D. Bowman, and G. C. P. King (2006), An observational test of the origin of accelerating moment release before large earthquakes, *J. Geophys. Res.*, *111*, B11304, doi:10.1029/2006JB004374.

1. Introduction

[2] It is generally accepted that large earthquakes strongly perturb the background seismicity rate in large regions. The most obvious of these perturbations are aftershocks, which are generally thought to be triggered by stress transferred from the main shock [e.g., *Karakostas et al.*, 2003, 2004; *King et al.*, 1994; *Toda and Stein*, 2002; *Wang and Chen*, 2001] and may persist for years to decades after a great event [e.g., *Utsu*, 1961]. There is also mounting evidence that "stress shadows" from large events can also depress the seismicity rate over broad regions [e.g., *Harris and Simpson*, 1996, 1998, 2002; *Ma et al.*, 2005; *Nalbant et al.*, 1998; *Pollitz et al.*, 2004; *Toda and Stein*, 2003]. In contrast, both observational and theoretical studies suggest that seismicity rate changes before large earthquakes are not as clearly defined. Various workers have documented evidence of both quiescence [e.g., *Wiemer and Wyss*, 1994; *Katsumata and Kasahara*, 1999; *Ogata*, 2005] and activation [e.g., *Bufe and Varnes*, 1993; *Jaumé and Estabrook*, 1992; *Knopoff et al.*, 1996] of regional seismicity before large events.

[3] Although the importance of precursory quiescence was recognized by workers as early as [*Mogi*, 1969], relatively few studies in recent years have explored this phenomenon [e.g., see *Holliday et al.*, 2006; *Ogata*, 2005; *Tiampo et al.*, 2006]. This is primarily due to the difficulty of obtaining statistically significant results over timescales of months or years. Instead, recent work on precursory seismicity rate changes before large earthquakes has focused on observations of increased seismic activity over a broad region, known as "accelerating moment release" (AMR). The earliest studies of accelerating moment release documented seismicity rate changes in the San Francisco Bay region [*Bufe and Varnes*, 1993; *Sykes and Jaumé*, 1990]. Since then, studies have documented AMR in a variety of regions, including California [*Bowman et al.*, 1998; *Bowman and King*, 2001; *Knopoff et al.*, 1996; *Sammis et al.*, 2004], Turkey and the Aegean [*Karakaisis et al.*, 2002, 2004; *Papazachos and Papazachos*, 2000; *Papazachos et al.*, 2002a, 2002b, 2002c], New Zealand [*Robinson*, 2000], the central United States [*Brehm and Braile*, 1998], Alaska [*Bufe et al.*, 1994; *Jaumé and Estabrook*, 1992], and Sumatra [*Jiang and Wu*, 2005; *Mignan et al.*, 2006].

[4] Two broad classes of models have been proposed to explain the origin of accelerating moment release before large earthquakes. Several authors have suggested that AMR is the result of a cascade of small earthquakes progressively building up stress before a large event [e.g., *Bowman and Sammis*, 2004; *Helmstetter and Sornette*, 2003; *Helmstetter et al.*, 2003; *Jaumé and Sykes*, 1999; *Saleur et al.*, 1996; *Sammis and Smith*, 1999; *Smalley et al.*, 1985; *Sornette and Sornette*, 1990; *Sornette and Sammis*, 1995]. In this view, the primary interaction is static stress

[1] Laboratoire Tectonique, Institut de Physique du Globe de Paris, Paris, France.
[2] Department of Geological Sciences, California State University, Fullerton, California, USA.

0148-0227/06/2006JB004374$09.00

transfer, and the accelerating activity is due to the self-organization of the stress field in a process similar to a phase transition [e.g., *Smalley et al.*, 1985; *Sornette and Sornette*, 1990]. In contrast, *King and Bowman* [2003] suggested that AMR is a secondary result of the loading of a large fault primarily by aseismic creep on the fault in the lower crust. In their so-called "stress accumulation" model, the accelerating activity is associated with a small amount of stress release in a volume of crust surrounding the future earthquake during the progressive loading of the main fault prior to a major earthquake.

[5] In this paper, we test the model of *King and Bowman* [2003] using observed seismicity in central and southern California. Because the loading process described by *King and Bowman* [2003] produces a spatially heterogeneous stress field (Figure 1), the AMR predicted by the model should be concentrated in regions determined by the geometry of the eventual main shock. Therefore a technique that uses the mechanism of the main shock to constrain the region where accelerating seismicity is observed [e.g., *Bowman and King*, 2001] should provide better constraints on the observation than a technique that ignores the mechanics of fault loading [e.g., *Bowman et al.*, 1998]. To test this hypothesis, we use the seismicity catalog for central and southern California to search for AMR before events $M \geq 6.5$ since 1950, similar to the studies of *Bowman et al.* [1998] and *Bowman and King* [2001]. Unlike the earlier studies, the seismicity catalog is first declustered to minimize spurious results in the pattern recognition algorithm. The procedure of *Bowman et al.* [1998] is then used to find a circular region that optimizes the observed AMR. Finally, the backslip model of *Bowman and King* [2001] is adopted to discriminate the regions within the circular area where seismicity should be increasing due to loading from below. If the stress accumulation model of *King and Bowman* [2003] is correct, then accelerating seismicity should be found preferentially in the regions identified by this procedure. However, if the events causing the AMR are distributed either preferentially in the negative lobes or randomly throughout the circular region then another mechanism, such as stress triggering, must play an important role in the origin of AMR. Although earlier work has addressed this topic qualitatively for selected events [e.g., *Sammis et al.*, 2004], this is the first study that systematically addresses both the importance of correctly identifying the loading regions when studying AMR and the relative role of stress triggering versus stress loading.

2. Methods

2.1. Quantifying AMR

[6] Seismicity rate changes are typically modeled by a simple power law time-to-failure equation [e.g., *Bufe and Varnes*, 1993]. This is a relation of the form

$$\varepsilon(t) = A + B(t_f - t)^m \quad (1)$$

where t_f is the time of the large event, B is negative and $m = 0.3$. A is the value of $\varepsilon(t)$ when $t = t_f$. The cumulative Benioff strain at time t is defined as

$$\varepsilon(t) = \sum_{i=1}^{N(t)} E_i(t)^{1/2} \quad (2)$$

where E_i is the energy of the ith event and N(t) is the number of events at time t. This phenomenon, known as Accelerating Moment Release, has been identified for a substantial number of earthquakes [e.g., *Sykes and Jaumé*, 1990; *Bowman et al.*, 1998; *Bowman and King*, 2001; *Bowman and Sammis*, 2004; *Jaumé and Sykes*, 1999; *Papazachos and Papazachos*, 2000].

[7] We use the algorithms originally developed by *Bowman et al.* [1998] to identify domains of accelerating seismicity. In order to quantify the degree of acceleration, *Bowman et al.* [1998] define a curvature parameter C (c value), where

$$C = \frac{(\text{powerlaw fit RMS error})}{(\text{linearlaw fit RMS error})} \quad (3)$$

Therefore, when the data are best characterized by a power law curve, the parameter C will be small. Following the approach of *Bowman et al.* [1998], the exponent m of equation (1) is held constant at 0.3. As a result, when the seismicity is either decelerating or linearly increasing C will be at or near unity, whereas accelerating sequences will have $C < 1$.

[8] In this study we use a Levenberg-Marquardt least squares routine to fit the seismicity data to equation (1). *Vere-Jones et al.* [2001] pointed out that the least squares technique leads to instabilities in the determination of the parameters of equation (1). However, they also note that the least squares method will produce a "reasonable visual fit to the data". In this work, the purpose of equations (1) and (2) are merely to provide a logical metric that can be used to identify accelerating activity in the seismicity data. Because the stress accumulation model of *King and Bowman* [2003] does not specify the precise functional form of accelerating moment release, the power law time to failure is used in this paper both for convenience and to be consistent with previous work.

2.2. Region Optimization

[9] To detect accelerating moment release in catalog data, it is necessary to isolate the precursory events in a space/time/magnitude window defined by the model of interest. Many studies use simple geometrical shapes such as circles [*Bowman et al.*, 1998; *Brehm and Braile*, 1998; *Robinson*, 2000; *Zöller et al.*, 2001] or ellipses [*Karakaisis et al.*, 2002; *Papazachos and Papazachos*, 2000] to define the region of interest. The C value provides a simple, computationally inexpensive parameter that can be used to optimize this region. Typically, a search algorithm finds the size and/or orientation of the region that produces the lowest C value, which is then defined as the precursory region. *Bowman and King* [2001] extended this technique to search for precursory regions defined by a backslip model for the loading region. In their technique, the region is optimized by searching for the contour of the backslip stress field within which the seismicity produces the lowest C value. *Sammis et al.* [2004] further refined the technique to search for both the best backslip loading region and the duration of the acceleration.

[10] Since the far-field stress distribution before a large earthquake is fully described by a backslip dislocation loading model, *Bowman and King* [2001] suggested that it

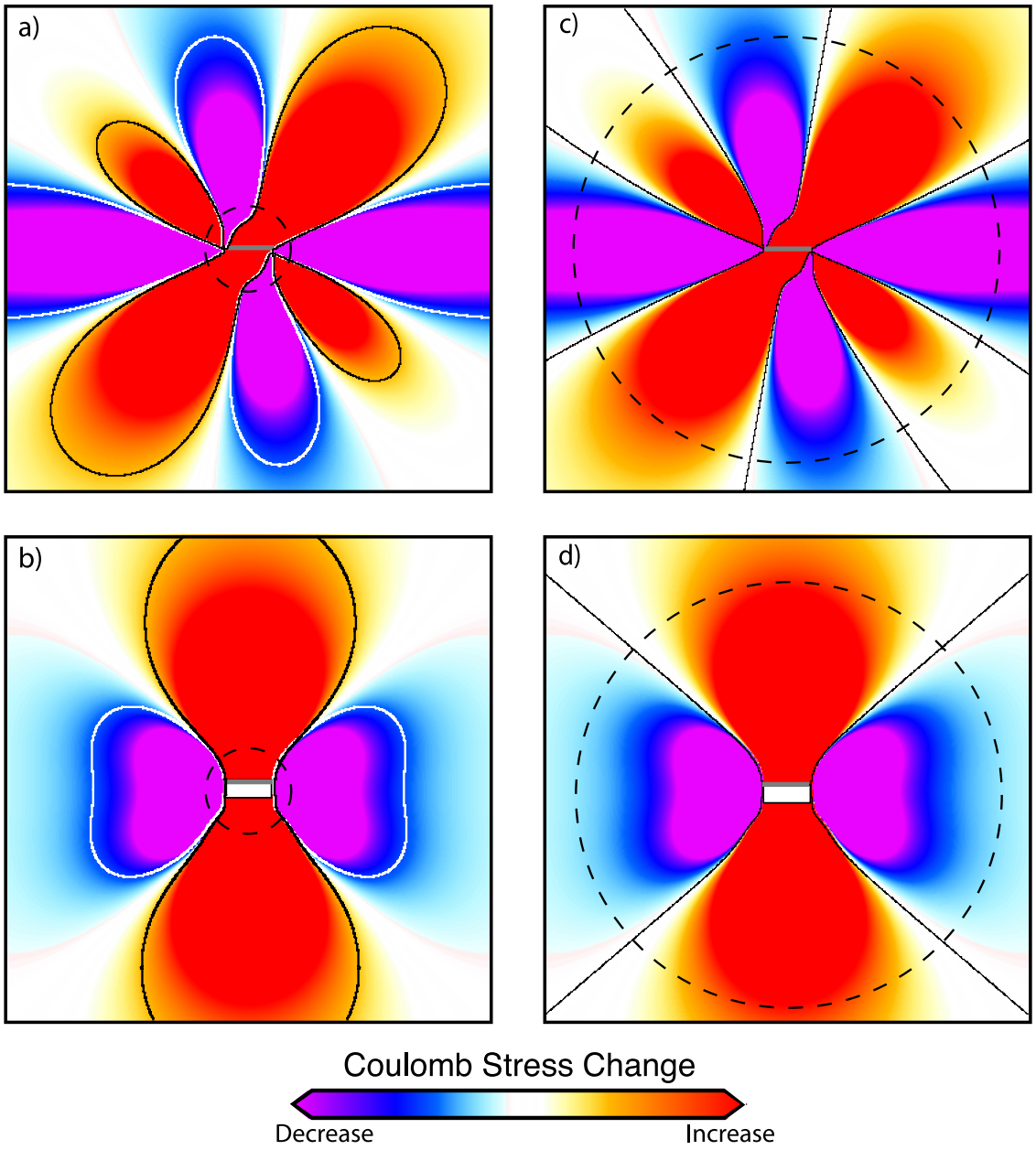

Figure 1. Stress distribution prior to (a and c) strike-slip and (b and d) dip-slip earthquakes calculated by the backslip method. This fully describes the far-field stress distribution used in the stress accumulation model. Although the near-field stresses may not be completely represented in regions where dip-slip faulting modifies the topography [e.g., *King et al.*, 1988; *Stein et al.*, 1988], the affected region is never larger than the area indicated by small dashed circles in Figures 1a and 1b and has no significant influence on the AMR studies discussed here. In earlier papers [e.g., *Bowman and King*, 2001; *Mignan et al.*, 2006; *Sammis et al.*, 2004], AMR was sought by finding an optimum stress contour (black line) in the lobes that must be loaded prior to the earthquake For each event a regional stress is chosen to be consistent with the mechanism of the main shock (Table 1). The actual value of the optimum stress is not important in this procedure. The loading model is only important to provide the azimuthal distribution defining where AMR is expected. In this paper, AMR is first optimized for circles. The dashed circles (Figures 1c and 1d) indicate a typical radius within which AMR is found. The black lines correspond to the zero stress contour and are used to distinguish the parts of the circular region enclosing events that reduce or increase stress on the future earthquake fault. In Figures 1a and 1c, the motion is left-lateral strike slip on a vertical fault (grey line), and in Figures 1b and 1d reverse motion occurs on a 45° dipping fault (outlined).

Table 1. Characteristics of All Earthquakes of $m \geq 6.5$ in Central and Southern California Between 1950 and 2000 and Their AMR Search Parameters

	Main Shock Source Parameters						Regional Stress Orientation		AMR Region	
Earthquake	Date	Mag	Strike	Dip	Length, km	Width, km	σ_1	σ_3	Δt, years	Radius, km
Kern County	21 Jul 1952	7.5	60	60	70	15	−30	60	9.75	102
Borrego Mountain	8 Apr 1968	6.5	135	90	30	20	0	90	22.44	23
San Fernando	9 Feb 1971	6.6	125	25	20	15	35	125	14.76	150
Coalinga	2 May 1983	6.7	135	15	38	7	45	135	47.84	90
Superstition Hills	24 Nov 1987	6.6	130	90	28	15	−5	85	5.72	136
Loma Prieta	18 Oct 1989	7.0	135	90	17	20	0	90	56.80	200
Landers	28 Jun 1992	7.3	150	90	80	15	15	105	35.05	212
Northridge	17 Jan 1994	6.7	120	35	20	15	30	120	37.45	231
Hector Mine	14 Oct 1999	7.1	145	90	50	15	10	100	47.93	228

provides a better identification of the precursory region than simple circular regions. They documented that this technique yields lower C values for accelerating sequences in the resulting regions. However, because *King and Bowman* [2003] demonstrated that the loading process should also produce regions where the seismicity rate is unchanged or even decreasing, a better test would be to assess the spatial distribution of the events contributing to the observed AMR. Figure 1 illustrates this concept for a simple vertical strike-slip fault and a 45° dipping reverse fault. A precursory region of interest defined by the backslip model of *Bowman and King* [2001] (black line in Figures 1a and 1c) will select events in the area where the stress accumulation model of *King and Bowman* [2003] shows the greatest increase in background seismicity. In contrast, the low-stress regions in the backslip model (outlined in white on Figures 1a and 1c) include the regions where *King and Bowman* [2003] predict AMR should not be observed. Therefore a simple test of the model would be to compare the C value of the AMR in these two regions.

[11] Such an approach is incorrect for two main reasons. First, the test implicitly assumes that the precursory seismicity must be within either the back or white contours in Figures 1a and 1c. This will not be the case if the signal is distributed throughout an arbitrary volume (e.g., in a circular region). Second, this approach creates an inherent procedural bias. In the most straightforward application, the regions to be compared would be defined by the equivalent "positive" and "negative" contours of the backslip stress field. However, this value is found by optimizing the contour in the positive lobes of the backslip stress field. This could be solved by also optimizing the negative lobes. However, this would result in the comparison of fundamentally different data sets. To avoid this procedural bias, any test of the distribution of seismicity should not include optimization of the stress field.

[12] In this study, AMR is identified in circular areas using the region optimization algorithm of *Bowman et al.* [1998]. The region of interest is found by calculating the C value in concentric circular regions up to 500 km in radius centered on the main shock epicenter. The duration of the AMR signal is also optimized as described by *Sammis et al.* [2004]. For each region radius, the beginning of the of the AMR signal is found by calculating the C value at an array of starting times ranging from the beginning of the catalog (see catalog description below) until the year prior to the event. The precursory region is defined as the combination of region radius and starting time that produces the optimal (lowest) C value. After the precursory region is defined, we apply the backslip model of *Bowman and King* [2001] to identify the subset of the circular region that was loaded by slip at depth (Figures 1b and 1d). Because the region size under consideration is much greater than the thickness of the seismogenic crust, the region optimization is effectively a two-dimensional (2-D) problem [*Bowman and King*, 2001]; the Coulomb stress fields used in this study are calculated on optimally oriented planes at a depth of 5 km with a coefficient of friction of 0.5. The source mechanism used for each event is listed in Table 1. With this approach, the identified precursory region is not dependent on any physical model, and event discrimination using the calculated stress field only occurs after optimization of the AMR. If slip at depth is the primary mechanism driving the observed AMR, then the C value for events in the positive prestress subregion should be significantly lower than the C value in the negative prestress subregion.

2.3. Statistical Significance

[13] Given sufficiently flexible search parameters, most optimization techniques designed in this manner will find some degree of acceleration in catalog data. We have quantified this bias by using random synthetic seismicity catalogs to determine the likelihood that a seismicity sequence with any given C value could have arisen stochastically [*Bowman et al.*, 1998]. We use a Monte Carlo approach, where 1000 catalogues each composed of 500 events placed randomly in space and time are created. The events are assigned a uniformly distributed random "longitude" and "latitude" in the range [0:1] and a uniformly distributed random time in the range [0:1]. Each point is indexed to a magnitude that respects the Gutenberg-Richter law in the magnitude range [3.5:6.0]. Energy for each point is calculated using the magnitude-energy scaling law ($E = 10^{4.8+1.5*M}$) developed by *Kanamori and Anderson* [1975]. This is then used to generate the cumulative Benioff strain curve. We test the false alarm rate in circular regions determined by the same search algorithm used for the California seismicity catalogue. For each synthetic catalog, the AMR search is done within concentric circles centered on the point (0.5, 0.5). The C value is calculated for regions with radii ranging from [0.05: 0.5] and starting times ranging from [0.0:0.90]. AMR cannot be reliably observed in regions containing fewer than five events. The optimization scheme automatically rejects these regions by assigning

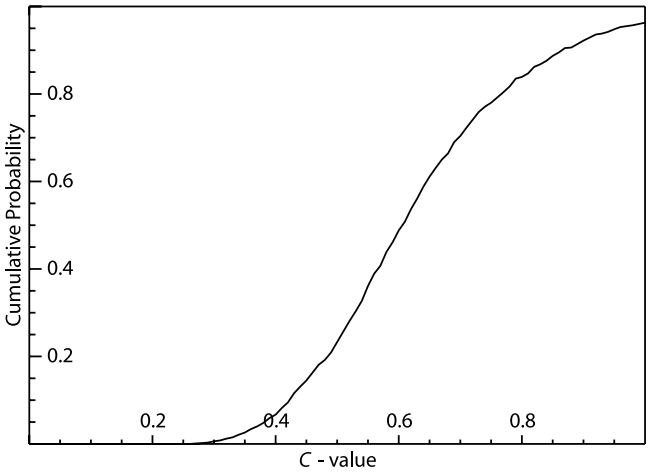

Figure 2. Cumulative probability of generating a given C value by stochastic processes. The plot suggests that any given synthetic catalog had a 50% chance of generating an optimal $C \geq 0.6$ and a 25% chance of generating $C \leq 0.5$.

them a C value of 1. The best (i.e., minimum) C value from the search is kept and the process is repeated for a new synthetic catalog.

[14] Figure 2 shows the result of this analysis expressed as the cumulative probability of observing a given C value or higher in the random synthetic catalog. Figure 2 suggests that any given synthetic catalog had a 50% chance of generating an optimal C value of 0.6 or higher. In contrast, the optimization procedure found $C \leq 0.5$ in less than 25% of the cases, and $C \leq 0.4$ in less than 7% of the synthetic catalogs. Because there is a high likelihood of generating $C \geq 0.6$ through stochastic processes, any seismicity sequence with $C \geq 0.6$ is classified in this study as having "unclear" AMR. Lower C values are more likely to represent AMR driven by nonrandom processes. We also note that these synthetic seismicity tests only produce stable C values for subregions with more than 25 events.

3. Data

[15] To facilitate comparison with earlier studies, we will analyze AMR before the nine $M \geq 6.5$ earthquakes in southern and central California studied by *Bowman and King* [2001] (Table 1). The seismicity catalog is provided by

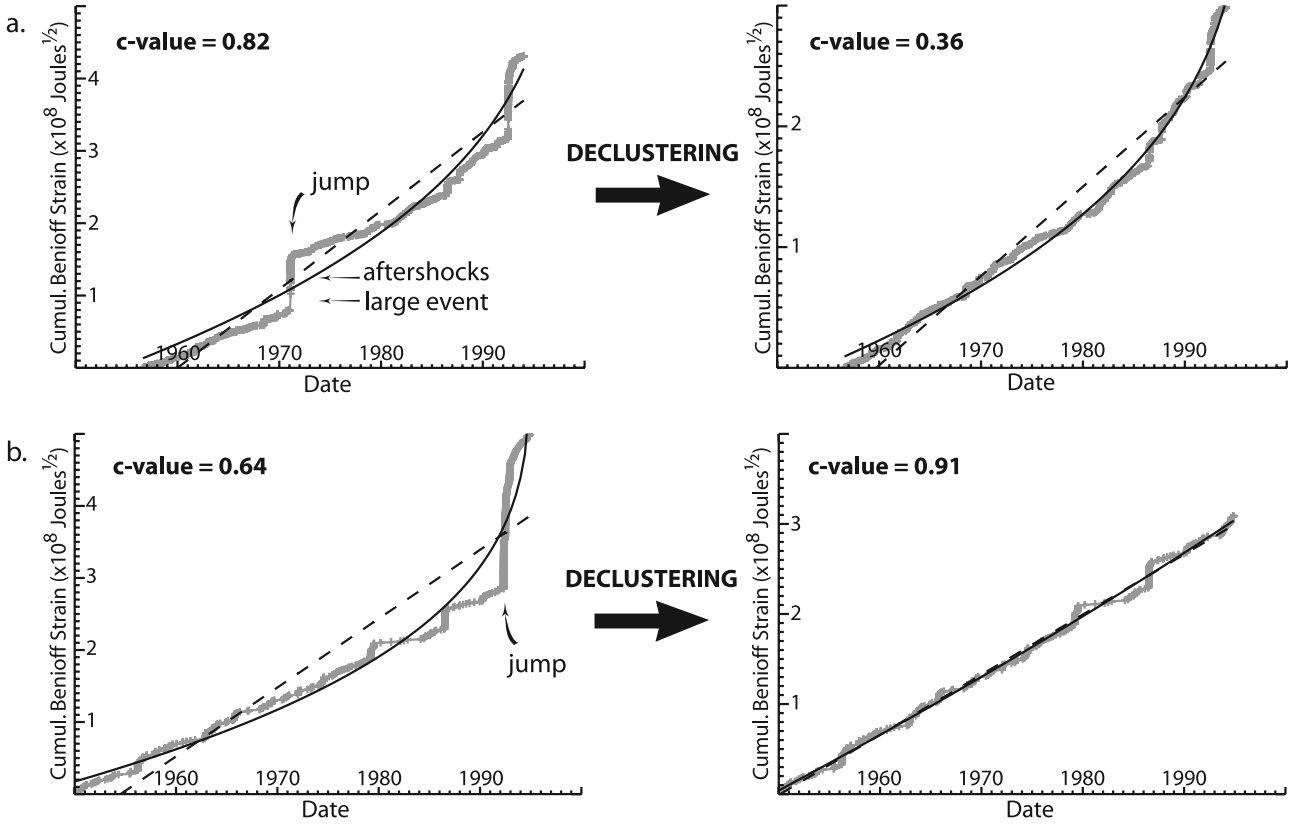

Figure 3. Influence of the declustering procedure on the calculation C. (a) A major jump in 1971 (San Fernando earthquake and its aftershocks) obscures the background acceleration ($C = 0.82$). Once major events ($m \geq 6.4$, see Appendix A) and their associated aftershocks are removed, the C value ($C = 0.36$) provides a better reflection of changes in the background seismicity rate. (b) Aftershocks cause a jump in the cumulative Benioff strain curve. The C value for this sequence is low ($C = 0.64$), even though the background seismicity is clearly not accelerating. After declustering the sequence gives $C = 0.91$, more consistent with the linear trend of the background seismicity.

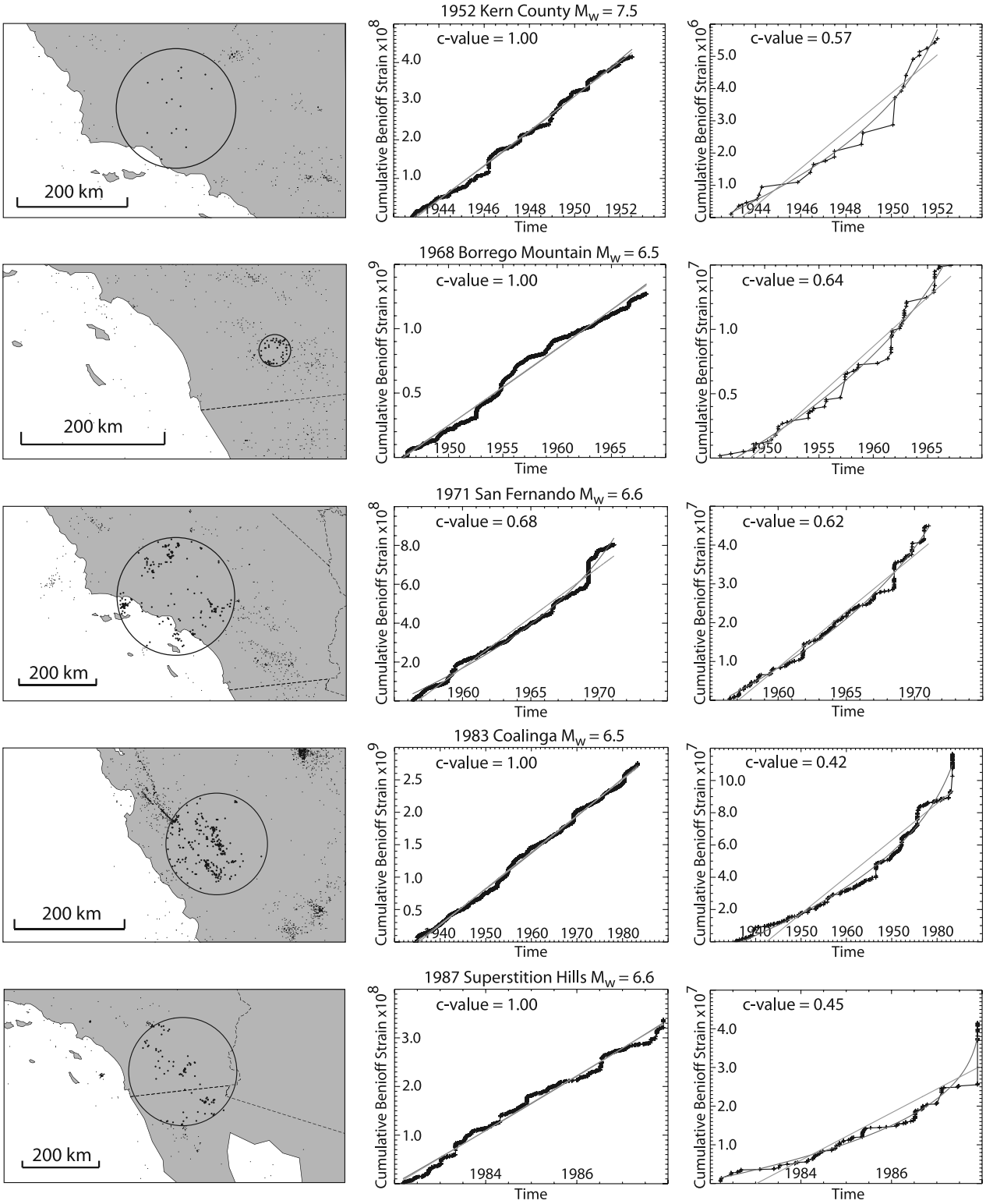

Figure 4a. Results for the AMR search by circles. (left) Optimal circular regions for the Kern County, Borrego Mountain, San Fernando, Coalinga, Superstition Hills, Loma Prieta, Landers, Northridge, and Hector Mine earthquakes. (middle) Cumulative Benioff strain for the entire region from the beginning of the observed AMR until the time of the respective main shock. This curve should be linear, indicating that there is no systematic change in the completeness of the catalog for the selected magnitude and time windows. (right) Cumulative Benioff strain in the optimal circular region for each event.

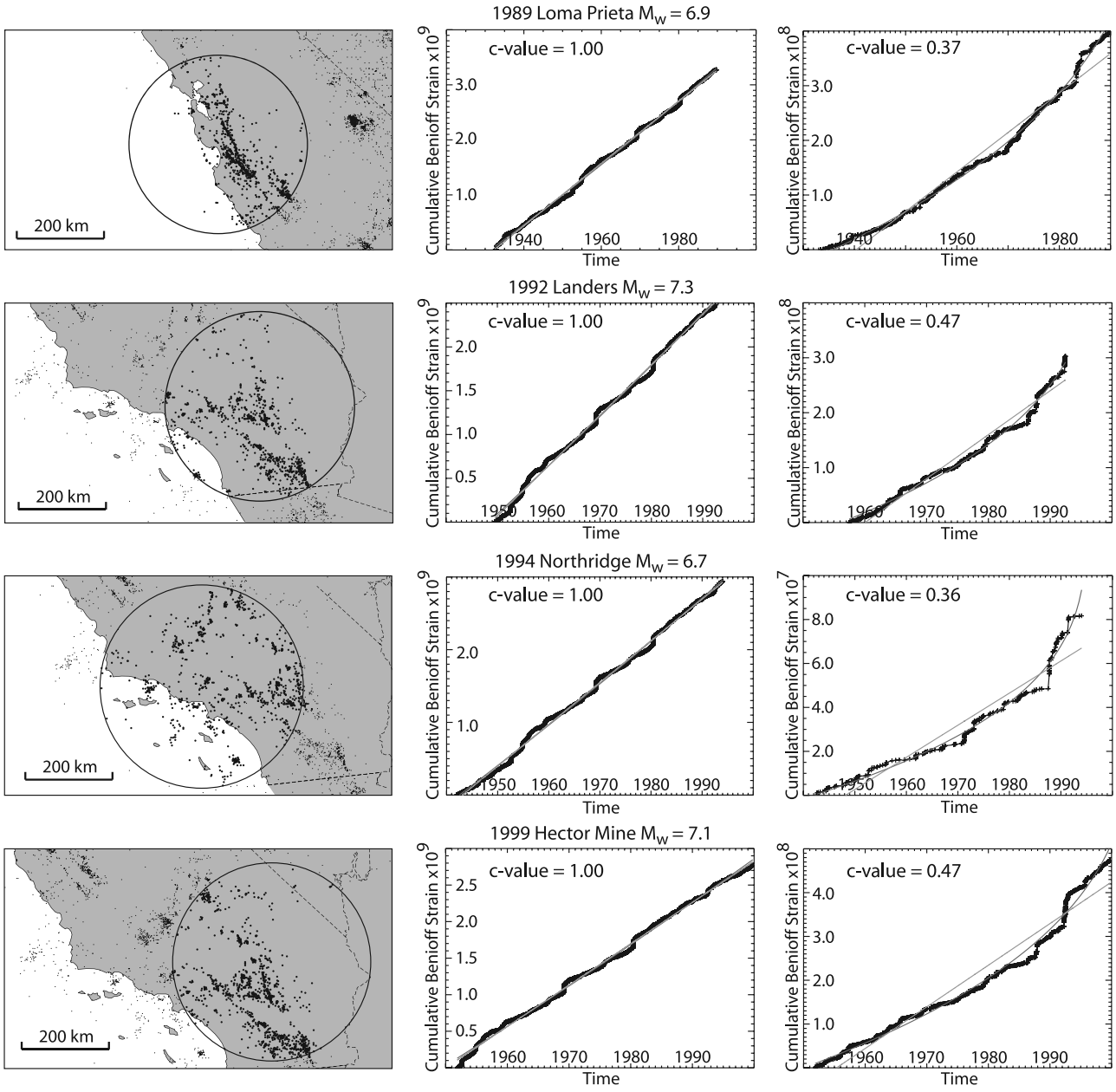

Figure 4b. Results for the AMR search by circles. (left) Optimal circular regions for the Kern County, Borrego Mountain, San Fernando, Coalinga, Superstition Hills, Loma Prieta, Landers, Northridge, and Hector Mine earthquakes. (middle) Cumulative Benioff strain for the entire region from the beginning of the observed AMR until the time of the respective main shock. This curve should be linear, indicating that there is no systematic change in the completeness of the catalog for the selected magnitude and time windows. (right) Cumulative Benioff strain in the optimal circular region for each event.

the Advanced National Seismic System (ANSS) (available athttp://quake.geo.berkeley.edu/anss/catalog-search.html). We used events larger than a magnitude threshold $m_0 = 3.5$ within the time window 1 January 1930 to 16 October 1999 (the date of the last M>6.5 event, Hector Mine). The AMR search was limited to a rectangular area 30° < latitude < 40° and −124° < longitude < −112°.

[16] Unlike previous studies of accelerating moment release, the seismicity catalog in this study was declustered prior to searching for AMR. Although the precise physical origin of aftershocks is still poorly understood, most explanations invoke some form of stress transfer (static and/or dynamic) from a larger event [*King and Cocco*, 2001; *King et al.*, 1994; *Stein*, 1999; *Toda and Stein*, 2000, 2002]. Because we are testing a model of seismicity rate changes driven by slip at depth, the unrelated transient effect of aftershocks will contaminate the results. Furthermore, the model of accelerating moment release described by *King and Bowman* [2003] results in a broad, steady increase of activity within the precursory region. Aftershocks to intermediate magnitude events in the precursory region represent a burst of activity that may produce

Table 2. C Values for All Earthquakes of $m \geq 6.5$ in Central and Southern California Between 1950 and 2000[a]

	C			
Earthquake	Region	Circle	Positive Stress	Negative Stress
Kern County	1.00	**0.57**	0.61	1.00
Borrego Mountain	0.94	0.64	0.63	1.00
San Fernando	0.93	0.62	**0.49**	0.93
Coalinga	1.00	**0.42**	**0.47**	0.63
Superstition Hills	1.00	**0.45**	**0.44**	1.00
Loma Prieta	1.00	**0.37**	**0.40**	0.62
Landers	1.00	**0.47**	**0.36**	0.65
Northridge	1.00	**0.36**	**0.47**	**0.54**
Hector Mine	1.00	**0.47**	**0.57**	0.80
Mean	0.99	**0.49**	**0.49**	0.80

[a]Values in bold correspond to reliable observations of accelerating moment release (AMR).

anomalous C values in the search algorithm (Figure 3). A detailed description of the declustering technique is provided in Appendix A.

[17] Changes in the lower magnitude of completeness of the catalog can cause artificial rate changes unrelated to any geologic process. In AMR studies, this generally is manifested as apparent acceleration through the entire catalog as the sensitivity of seismic networks improves. To evaluate this, the C value is calculated for the entire declustered catalog during the time window in which AMR is observed for the nine earthquakes being studied. In all nine cases, the evolution of the cumulative Benioff strain is clearly linear for the entire region ($C_{\text{mean}} = 0.96$) (see Figure 4a, 4b and Table 2).

4. Results and Discussion

[18] For each of the nine earthquakes studied, it was possible to find clear AMR in optimized circles centered on their epicenter ($C_{\text{mean}} = 0.49$, details in Table 2). The observed C values for the circular regions ranged from 0.36 for the 1994 Northridge earthquake to 0.64 for the 1968 Borrego Mountain event (Figures 4a and 4b). Note that the size of the regions found here are slightly different from those found by previous studies [e.g., *Bowman et al.*, 1998; *Zöller et al.*, 2001]. This is because the current study used declustered seismicity and the search algorithm jointly optimized the region size and the duration of the AMR.

[19] The backslip stress models of *Bowman and King* [2001] were next used to discriminate between the "positive" and "negative" prestress regions within each optimal circular region. Figures 5a and 5b shows the resulting regions and seismicity curves for each of the studied events. The dashed lines in Figure 5a represent the 0-bar stress change contour. The areas shaded dark grey are within the optimal circular radius and in the positive lobes of the prestress field; this is where the stress accumulation model of *King and Bowman* [2003] predicts seismicity leading to AMR should be concentrated. The light grey regions are within the optimal circular radius but in the negative lobe of the prestress field; *King and Bowman* [2003] predict that AMR in this region should be weak or nonexistent. The seismicity curves for the positive and negative prestress zones are shown in Figures 5a and 5b, respectively, and summarized in Table 2.

[20] In the positive prestress regions, C values range from $C = 0.36$ for the 1992 Landers earthquake to $C = 0.63$ for the 1968 Borrego Mountain event, with $C_{\text{mean}} = 0.49$. The seismicity in the positive stress regions produced AMR much more reliably than the random synthetic catalogs. Only two events had $C > 0.6$, Borrego Mountain ($C = 0.63$) and Kern County ($C = 0.61$); random catalogs have an approximately 50% chance of producing similar acceleration. Six of the events (San Fernando, Coalinga, Superstition Hills, Loma Prieta, Landers, and Northridge) had $C < 0.5$; random catalogs have less than 23% chance of producing any of these individual sequences. The probability of random catalogs producing all of these sequences is small.

[21] The negative prestress region had C values ranging from 0.54 for the 1994 Northridge earthquake to $C = 1.0$ for the 1952 Kern County, 1967 Borrego Mountain, and 1987 Superstition Hills events, with $C_{\text{mean}} = 0.80$. Only one event had $C < 0.6$ (Northridge).

[22] We note that the circular search by itself appears to outperform the model of *Bowman and King* [2001]. Furthermore, the regions found here are significantly different from those observed in earlier work [e.g., *Bowman et al.*, 1998; *Bowman and King*, 2001]. However, a direct comparison between earlier work and the results of this paper is not possible for two main reasons. First, *Bowman and King* [2001] performed an optimization of the stress contour used to define the region of interest, whereas no optimization of the stress field was permitted here. Second, *Bowman and King* [2001] did not decluster the seismicity, unlike the data used in this study. Therefore the results of this study should not be interpreted to indicate that circular regions outperform the backslip loading model.

[23] What do these results suggest about the physical mechanism driving observed accelerating moment release before large earthquakes? If cascading interactions driven by stress transfer from smaller events is the driving mechanism of AMR, then the precursory rate changes should be expected to be strongest in the negative lobes of the Coulomb prestress field. In contrast, if the stress accumulation model of *King and Bowman* [2003] is correct, then AMR should be more apparent (smaller C values) in the positive lobe of the prestress field. The latter prediction is true for all nine earthquakes in the study region, consistent with the predictions of *King and Bowman* [2003]. This suggests that slip at depth has a strong, if not dominant, influence on the development of accelerating moment release. While this alone does not rule out cascading seismicity as an important factor in the evolution of regional seismicity, it does suggest that static stress triggering does not play an important role in the generation of Accelerating Moment Release.

[24] The relative importance of stress triggering and stress loading in generating precursory AMR has implications not only for the spatial distribution of accelerating seismicity in the region of an impending earthquake, but also for the size of events that might be expected to exhibit precursory AMR. Simple static stress interaction models (Figure 6) demonstrate the relative role of stress triggering and stress loading for events with different ratios of fault length, L, to width, W. Figure 6 shows the fault plane viewed face-on, with a dotted rectangle indicating the site of an upcoming event. The grey region at the base of Figures 6a and 6b

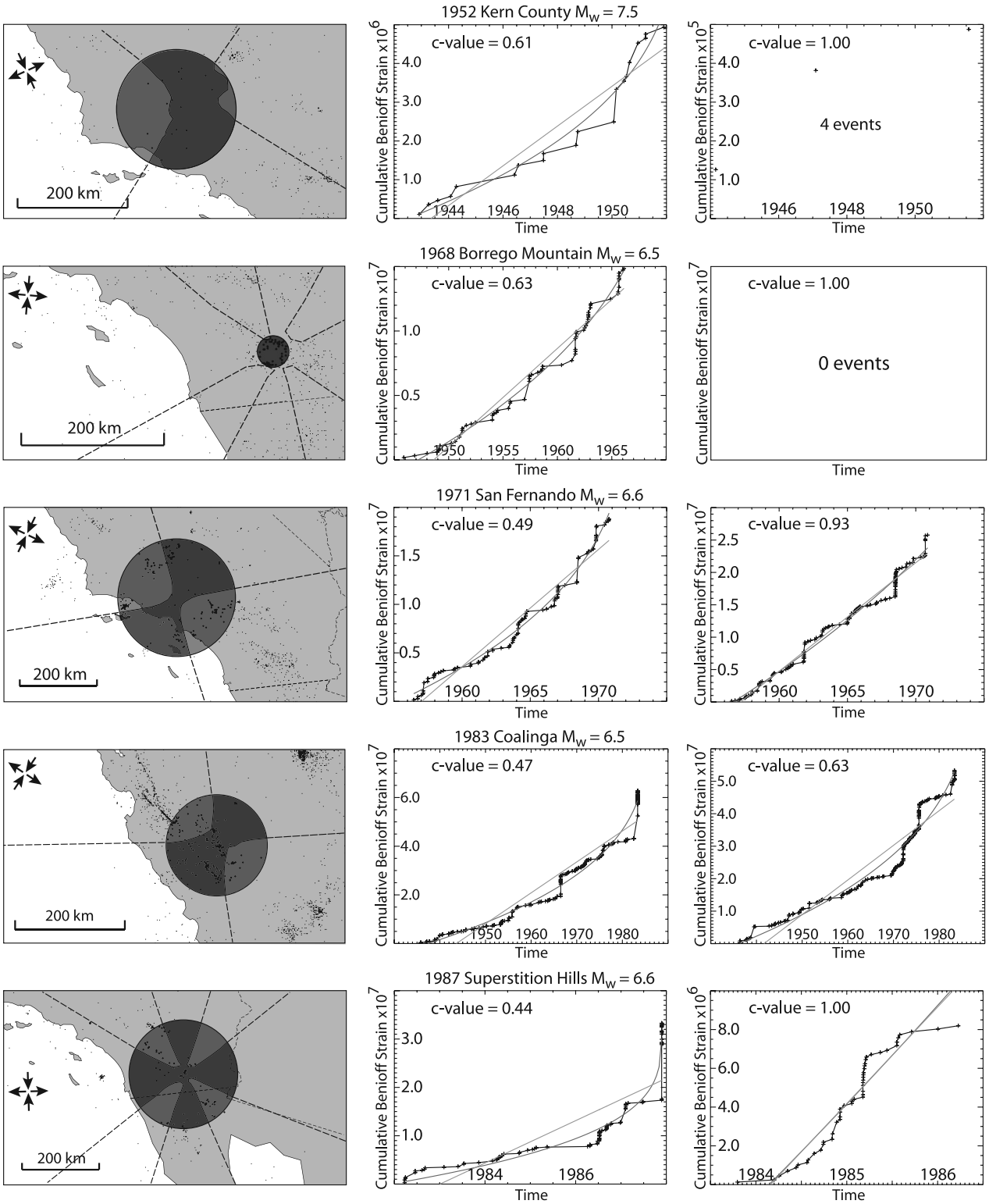

Figure 5a. Results for the AMR search by regions of positive and negative prestress. (left) Search regions. The optimal circular region (Figures 4a and 4b) is shown. The dashed line indicates the 0-bar stress change contour; regions of positive stress are shaded dark grey, and regions of negative stress are shaded light grey. The orientation of the regional stress field used to calculate the prestress is indicated by the arrows on the map. (middle) Cumulative Benioff strain in the positive stress regions. (right) Cumulative Benioff strain in the negative stress regions. See text for discussion.

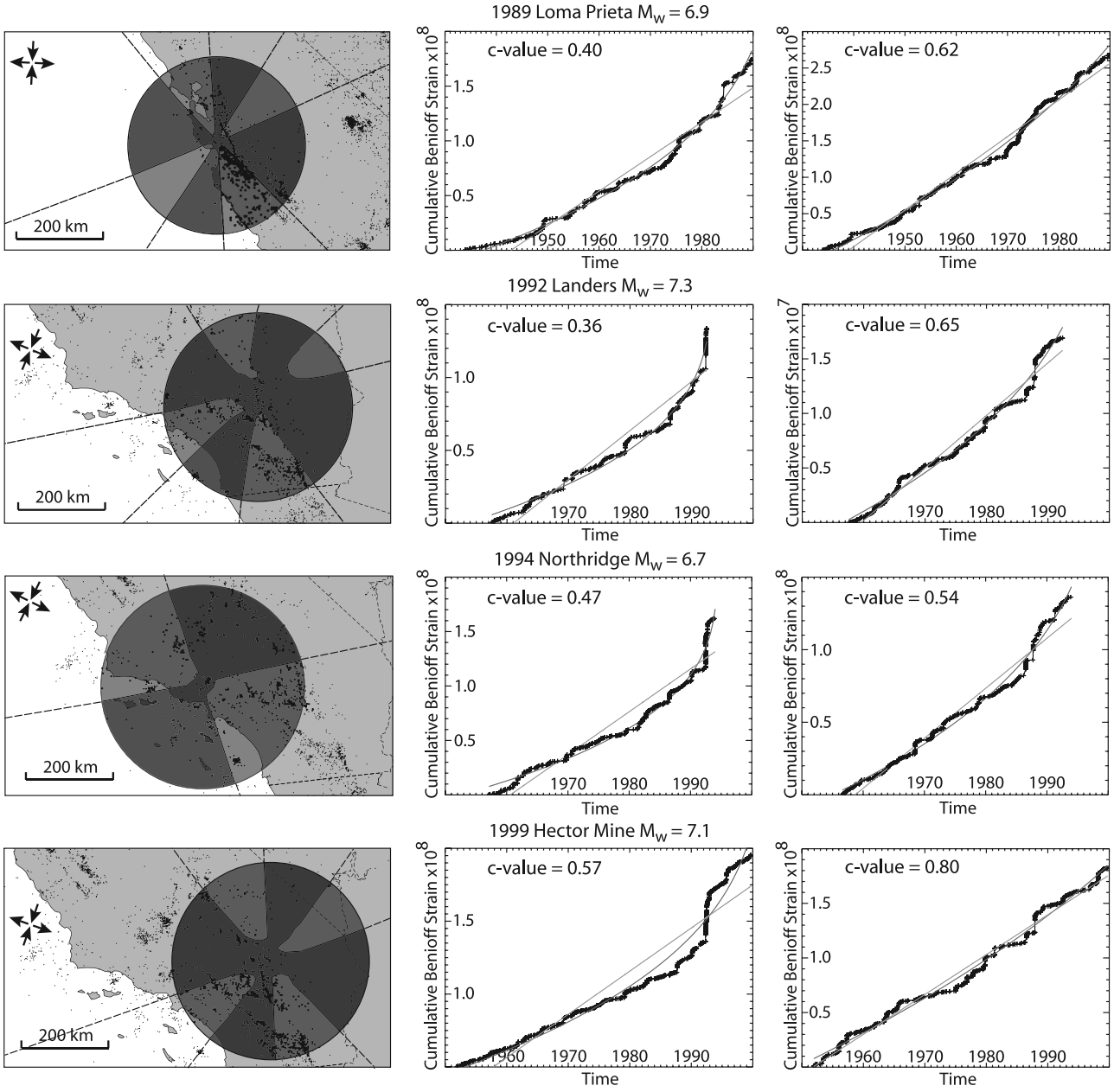

Figure 5b. Results for the AMR search by regions of positive and negative prestress. (left) Search regions. The optimal circular region (Figures 4a and 4b) is shown. The dashed line indicates the 0-bar stress change contour; regions of positive stress are shaded dark grey, and regions of negative stress are shaded light grey. The orientation of the regional stress field used to calculate the prestress is indicated by the arrows on the map. (middle) Cumulative Benioff strain in the positive stress regions. (right) Cumulative Benioff strain in the negative stress regions. See text for discussion.

represents the fault in the lower crust, which moves aseismically to load the overlying seismogenic portion of the fault. The white rectangles represent the rupture area of earlier events along strike with sizes comparable to the impending earthquake; the coloring represents the static stress change in the seismogenic zone from both the earlier adjacent events and creep on the fault in the lower crust.

[25] For events with L/W $\approx$ 1 (Figure 6a), stress transfer from adjacent events contributes more to the overall stress on the fault than the loading caused by aseismic creep in the lower crust. This can be seen by comparing the 10-bar stress contour for adjacent event (solid line) and the loading from below (dashed line). In contrast, the stress field on the fault plane of events with L/W > 1 (Figure 6b) is dominated by aseismic creep on the fault in the lower crust. Although static stress triggering certainly increases the stress on the plane of the impending earthquake, the effect is restricted to only a small section of the fault. Comparing the 10-bar stress contour for both the adjacent event and loading from below suggests that large earthquakes are dominantly loaded by aseismic slip on the fault at depth rather than stress transfer

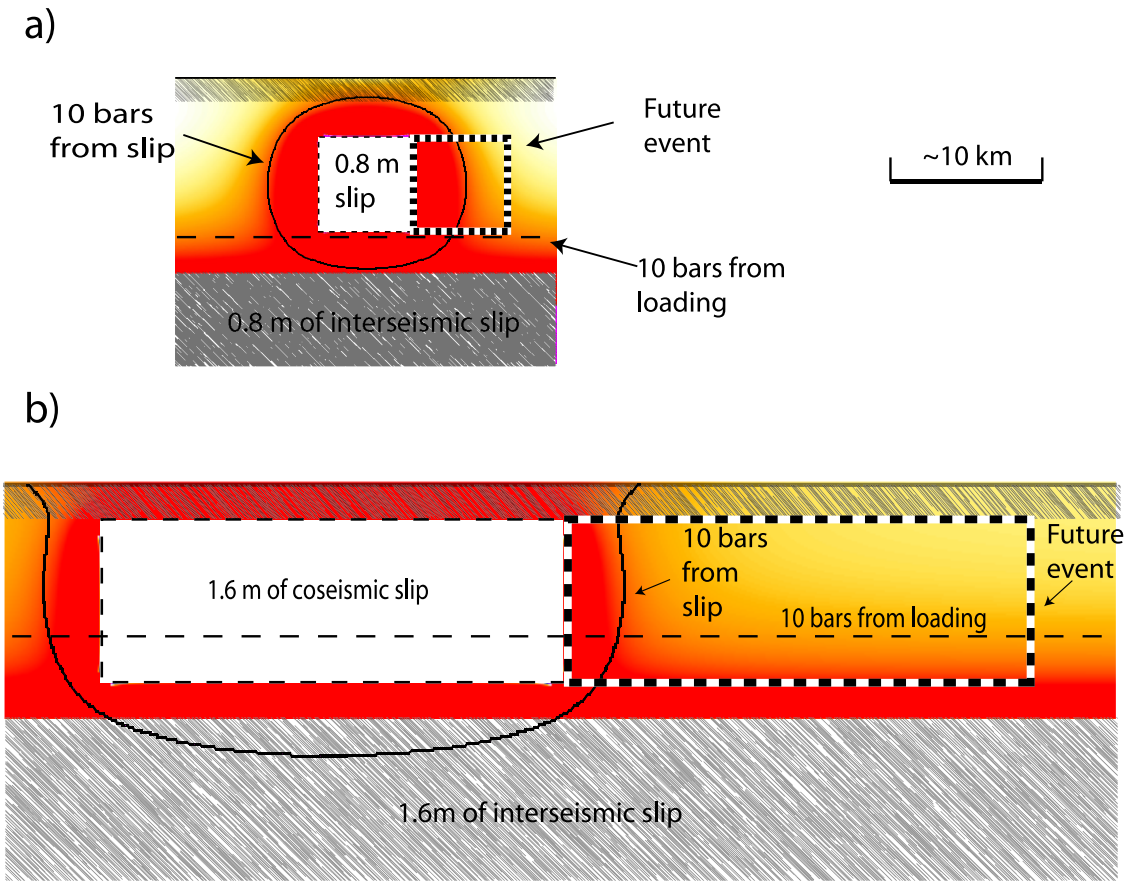

Figure 6. Role of stress triggering and stress loading for faults of different L/W ratios. The coloring indicates the stress level. In the models, a surface that has already ruptured (white rectangle) increases stress around it. Under the seismogenic zone, the fault (shaded grey) moves aseismically causing loading. The relative contribution of each effect can be assessed by looking at the 10 bar contour indicated for each separately. (a) For small events, L/W$\sim$1, the stress field on the fault plane may be weakly influenced by loading and greatly influenced by adjacent events. (b) For a large event (L/W > 1), loading predominates the stress field on the fault plane of the future event.

from nearby earthquakes, consistent with the results presented here.

[26] Because stress triggering is the dominant loading mechanism for small and intermediate (L/W $\approx$ 1) events, slip at depth will not necessarily be the dominant loading mechanism on the rupture plane of the small earthquakes. Unlike large events, it is likely that any precursory seismicity before small earthquakes is dominated by stress transfer. However, any systematic test of this concept for small events would require much higher precision catalog locations than are routinely available at present. Furthermore, the stress-based approach used in this work is not practical for small earthquakes since the focal mechanisms for these events are not well constrained in most earthquake catalogs. As a result, investigations of precursory activity for small-to-intermediate magnitude seismicity are more suitable using statistical techniques such as the Pattern Informatics method [e.g., *Tiampo et al.*, 2006].

[27] This simple model for the relative importance of stress triggering versus fault loading also suggests that the approach of *Bowman and King* [2001] can only be reliably used to observe AMR before large earthquakes. Furthermore, our results suggest that models of regional seismicity that are driven primarily by stress transfer and fail to account for loading by aseismic creep at depth [e.g., *Robinson et al.*, 2005] will not produce systematic accelerating moment release before model events. Because the loading mechanism for events with L/W > 1 is dominated by aseismic creep on the fault in the lower crust, seismicity rate changes before large earthquakes are more accurately represented by the model of *King and Bowman* [2003], as supported by the results of this study.

Appendix A: Declustering Algorithm

[28] Aftershocks represent a local perturbation of the background seismicity rate as the stress field is reorganized following an earthquake. This process is independent of the slow regional seismicity rate change represented by AMR. However, large aftershock sequences produce step function changes in the regional seismicity rate. This is evident in the cumulative Benioff strain plot for the entire California catalog shown in Figure A1a. The *C* value analysis described in the main text could incorrectly identify these

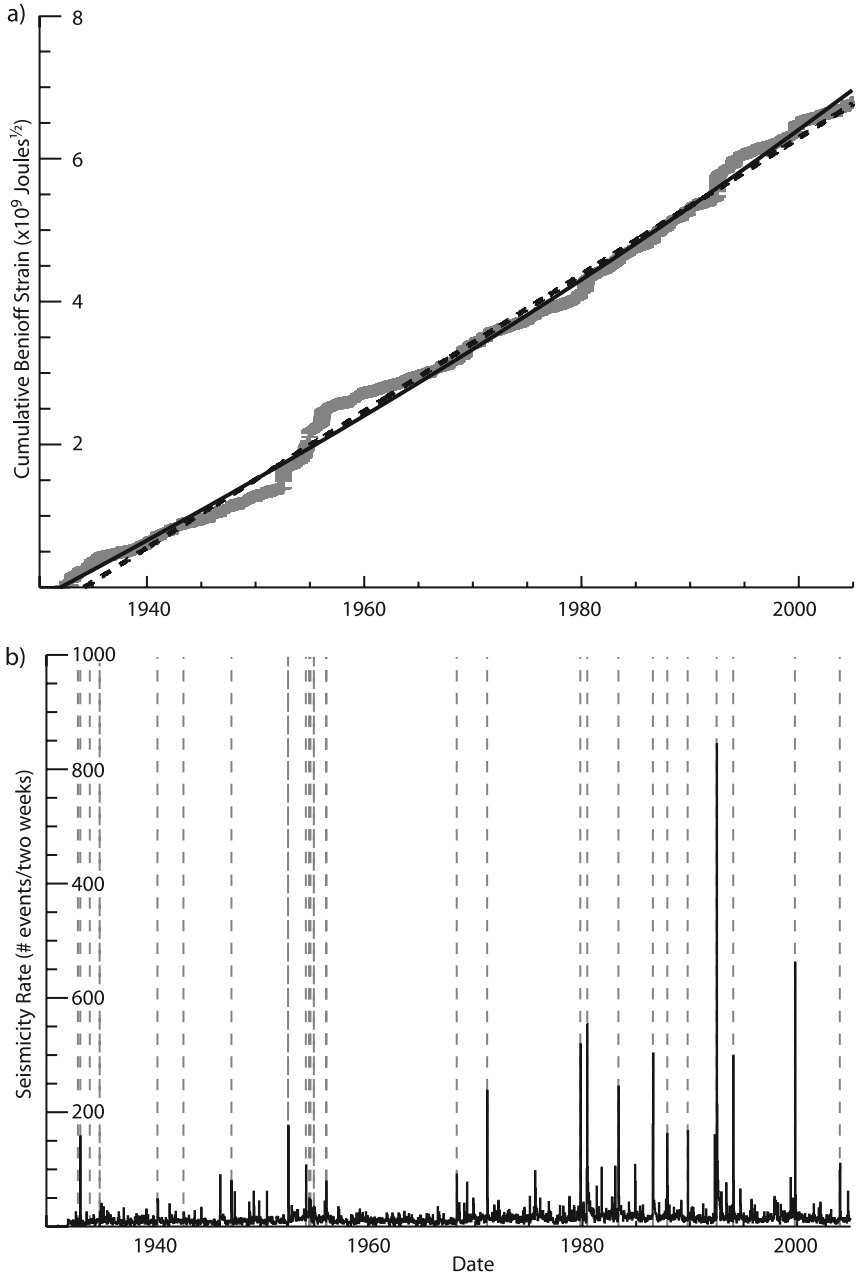

Figure A1. Seismicity catalogue for central and southern California (from 1930 to 2005) before declustering. (a) Evolution of the cumulative Benioff strain for the entire catalog. Note the irregularity of the curve, corresponding to the presence of large events and their associated aftershocks. (b) Seismicity rate through the duration of the catalog. The averaged number of events ($n \approx 17$) corresponds to the background seismicity for a period of 2 weeks (average background rate). The majority of the peaks in the seismicity rate can be related to the occurrence of $M \geq 6.4$ earthquakes.

aftershock clusters as AMR. To alleviate this problem, the seismicity catalog in this study is declustered before the C value analysis is run.

[29] The average seismicity rate is defined here as the number of events $M \geq 3.5$ in a 2-week window. For the duration of the catalog (Figure A1), the average seismicity rate defined in this way is 17 events per 2 weeks. We classify an event as part of an aftershock cluster if it (1) occurs when the seismicity rate is greater than the long-term average; (2) is preceded by an event greater than some arbitrary main shock threshold, M_{main}; and (3) is within some distance, $R_{cluster}$, of a main shock. For this study, $R_{cluster} = 50$ km. The main shock threshold, M_{main}, is a parameter that is adjusted to achieve the desired level of declustering for the catalog. For instance, the dashed lines in Figure A1b indicate the occurrence of $M \geq 6.4$ events in the catalog used here. By inspection, it is clear that most of the bursts in seismicity rate coincide with events $M \geq 6.4$. We therefore select $M_{main} = 6.4$ as the main shock threshold for the declustering. The declustering algorithm works by

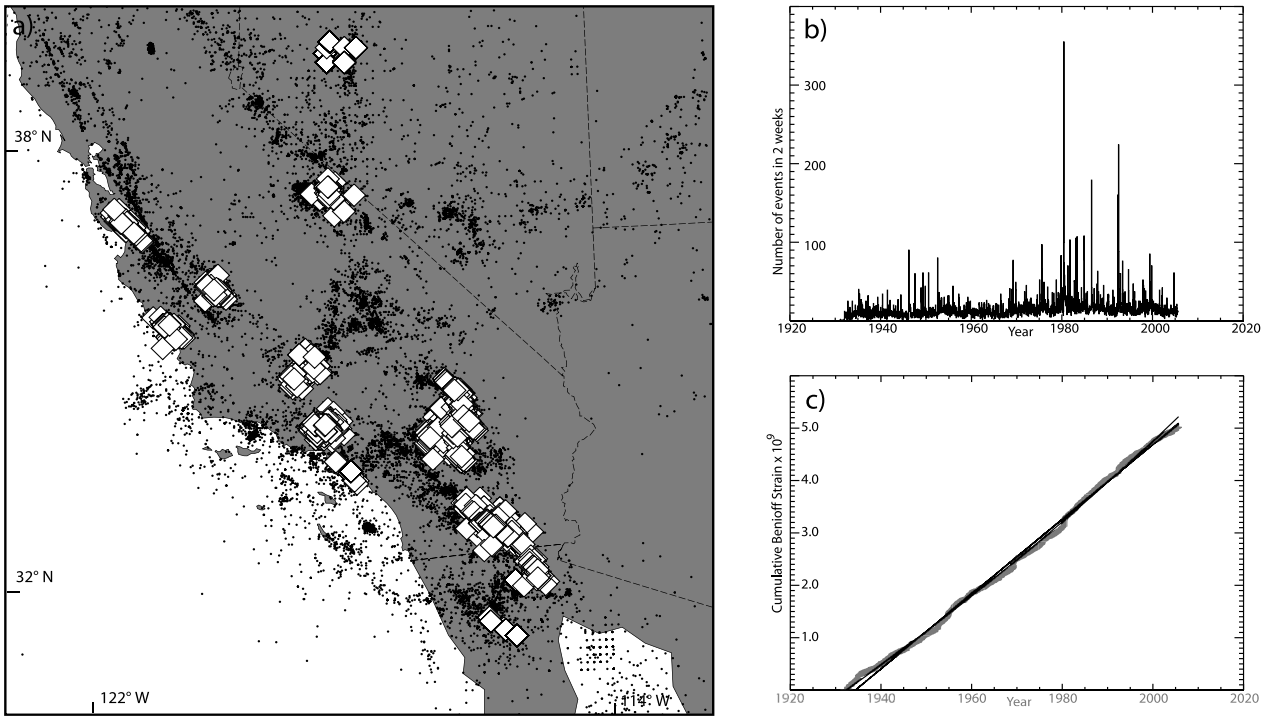

Figure A2. Declustered seismicity catalog. (a) Map of the region. White diamonds correspond to events that have been removed by the declustering procedure (see text for details). Each cluster is composed of a large event ($m \geq 6.4$) and its aftershocks. (b) Seismicity rate of the declustered catalog. Some high seismicity rate peaks are still present. These clusters are either swarms or are preceded by a $M < 6.4$ main shock and are left in the catalog. (c) Evolution of the cumulative Benioff strain in the entire declustered catalog. Note the relatively linear trend of the curve after declustering.

deleting all aftershocks until the seismicity rate is equal to the long-term average.

[30] The results of this declustering algorithm are shown in Figure A2. In the new catalogue, 4069 events have been removed (28 of $m \geq 6.4$) for a total of 31415 events. Figure A2a shows the mapped distribution of ''independent'' earthquakes (black dots) and deleted aftershocks (white diamonds). Figure A2b shows the seismicity rate of the declustered catalog. Note that not all of the clusters were removed. Our goal is not to identify all aftershocks, but to minimize their impact on the cumulative seismicity curves. An inspection of Figure A2c shows that this is the case; the steps in the curve caused by aftershocks have been removed, resulting in a smooth seismicity curve for the entire catalog. The same effect can be achieved with a wide range of declustering parameters.

[31] **Acknowledgments.** The authors acknowledge helpful reviews by Russell Robinson and Kristy Tiampo, as well as Associate Editor Steve Cohen. This research was supported by the INSU-CNRS and the Southern California Earthquake Center. SCEC is funded by NSF Cooperative Agreement EAR-0106924 and USGS Cooperative Agreement 02HQAG0008. This paper is IPGP contribution 2157, INSU contribution 393, and SCEC contribution 882.

References

Bowman, D. D., and G. C. P. King (2001), Accelerating seismicity and stress accumulation before large earthquakes, *Geophys. Res. Lett.*, *28*, 4039–4042.

Bowman, D. D., and C. G. Sammis (2004), Intermittent criticality and the Gutenberg-Richter distribution, *Pure Appl. Geophys.*, *104*, 1945–1956, doi:10.1007/s00024-004-2541-z.

Bowman, D. D., G. Ouillon, C. G. Sammis, A. Sornette, and D. Sornette (1998), An observational test of the critical earthquake concept, *J. Geophys. Res.*, *103*, 24,359–24,372.

Brehm, D. J., and L. W. Braile (1998), Intermediate-term earthquake prediction using precursory events in the New Madrid seismic zone, *Bull. Seismol. Soc. Am.*, *88*, 564–580.

Bufe, C. G., and D. J. Varnes (1993), Predictive modeling of the seismic cycle of the greater San Francisco Bay region, *J. Geophys. Res.*, *98*, 9871–9883.

Bufe, C. G., S. P. Nishenko, and D. J. Varnes (1994), Seismicity trends and potential for large earthquakes in the Alaska-Aleutian region, *Pure Appl. Geophys.*, *142*, 83–99.

Harris, R. A., and R. W. Simpson (1996), In the shadow of 1857-the effect of the great Ft. Tejon earthquake on subsequent earthquakes in southern California, *Geophys. Res. Lett.*, *23*, 229–232.

Harris, R. A., and R. W. Simpson (1998), Suppression of large earthquakes by stress shadows: A comparison of Coulomb and rate-and-state failure, *J. Geophys. Res.*, *103*, 24,439–24,452.

Harris, R. A., and R. W. Simpson (2002), The 1999 M_w 7.1 Hector Mine, California, earthquake: A test of the stress shadow hypothesis?, *Bull. Seismol. Soc. Am.*, *92*, 1497–1512, doi:10.1785/0120000825.

Helmstetter, A., and D. Sornette (2003), Foreshocks explained by cascades of triggered seismicity, *J. Geophys. Res.*, *108*(B10), 2457, doi:10.1029/2003JB002409.

Helmstetter, A., D. Sornette, and J. Grasso (2003), Mainshocks are aftershocks of conditional foreshocks: How do foreshock statistical properties emerge from aftershock laws, *J. Geophys. Res.*, *108*(B1), 2046, doi:10.1029/2002JB001991.

Holliday, J. R., J. B. Rundle, K. F. Tiampo, W. Klein, and A. Donnelan (2006), Modification of the pattern informatics method for forecasting large earthquake events using complex eigenfactors, *Tectonophysics*, *413*, 87–91.

Jaumé, S. C., and C. H. Estabrook (1992), Accelerating seismic moment release and outer rise compression: Possible precursors to the next great earthquake in the Alaska Peninsula region, *Geophys. Res. Lett.*, *19*, 345–348.

Jaumé, S. C., and L. R. Sykes (1999), Evolving towards a critical point: A review of accelerating seismic moment/energy release prior to large and great earthquakes, *Pure Appl. Geophys.*, *155*, 279–305.

Jiang, C. S., and Z. L. Wu (2005), The December 26, 2004, off the west coast of northern Sumatra, Indonesia, M_w = 9.0, earthquake and the critical-point-like model of earthquake preparation, *Acta Seismol. Sin.*, *18*, 290–296.

Kanamori, H., and D. L. Anderson (1975), Theoretical basis of some empirical relations in seismology, *Bull. Seismol. Soc. Am.*, *65*, 1073–1095.

Karakaisis, G. F., C. B. Papazachos, A. S. Savvaidis, and B. C. Papazachos (2002), Accelerating seismic crustal deformation in the North Aegean Trough, Greece, *Geophys. J. Int.*, *148*, 193–200, doi:10.1046/j.0956-540x.2001.01578.x.

Karakaisis, G. F., C. B. Papazachos, E. M. Scordilis, and B. C. Papazachos (2004), Current accelerating seismic excitation along the northern boundary of the Aegean Microplate, *Tectonophysics*, *383*, 81–89, doi:10.1016/j.tecto.2004.03.005.

Karakostas, V. G., E. E. Papadimitriou, G. F. Karakaisis, C. B. Papazachos, E. M. Scordilis, G. Vargemezis, and E. Aidona (2003), The 2001 Skyros, northern Aegean, Greece, earthquake sequence: Off-fault aftershocks, tectonic implications, and seismicity triggering, *Geophys. Res. Lett.*, *30*(1), 1012, doi:10.1029/2002GL015814.

Karakostas, V. G., E. E. Papadimitriou, and C. B. Papazachos (2004), Properties of the 2003 Lefkada, Ionian Islands, Greece, earthquake seismic sequence and seismicity triggering, *Bull. Seismol. Soc. Am.*, *94*, 1976–1981, doi:10.1785/012003254.

Katsumata, K., and M. Kasahara (1999), Precursory seismic quiescence before the 1994 Kurile earthquake (M_w = 8.3) revealed by three independent seismic catalogs, *Pure Appl. Geophys.*, *155*, 443–470.

King, G. C. P., and D. D. Bowman (2003), The evolution of regional seismicity between large earthquakes, *J. Geophys. Res.*, *108*(B2), 2096, doi:10.1029/2001JB000783.

King, G. C. P., and M. Cocco (2001), Fault interaction by elastic stress changes: New clues from earthquake sequences, *Adv. Geophys.*, *44*, 1–38.

King, G. C. P., R. S. Stein, and J. B. Rundle (1988), The growth of geological structures by repeated earthquakes: 1. Conceptual framework, *J. Geophys. Res.*, *93*, 13,307–13,318.

King, G. C. P., R. S. Stein, and J. Lin (1994), Static stress changes and the triggering of earthquakes, *Bull. Seismol. Soc. Am.*, *84*, 935–953.

Knopoff, L., T. Levshina, V. Keilis-Borok, and C. Mattoni (1996), Increased long-range intermediate-magnitude earthquake activity prior to strong earthquakes in California, *J. Geophys. Res.*, *101*, 5779–5796.

Ma, K.-F., C.-H. Chan, and R. S. Stein (2005), Response of seismicity to Coulomb stress triggers and shadows of the 1999 M_w = 7.6 Chi-Chi, Taiwan, earthquake, *J. Geophys. Res.*, *110*, B05S19, doi:10.1029/2004JB003389.

Mignan, A., G. C. P. King, D. D. Bowman, R. Lacassin, and R. Dmowska (2006), Seismic activity in the Sumatra-Java region prior to the December 26, 2004 (M_w = 9.0–9.3) and March 28, 2005 (M_w = 8.7) earthquakes, *Earth Planet. Sci. Lett.*, *244*, 639–654, doi:10.1016/j.epsl.2006.01.058.

Mogi, K. (1969), Some features of recent seismic activity in and near Japan (2), Activity before and after large earthquakes, *Bull. Earthquake Res. Inst. Univ. Tokyo*, *47*, 395–417.

Nalbant, S. S., A. Hubert, and G. C. P. King (1998), Stress coupling between earthquakes in northwest Turkey and the north Aegean Sea, *J. Geophys. Res.*, *103*, 24,469–24,486.

Ogata, Y. (2005), Detection of anomalous seismicity as a stress change sensor, *J. Geophys. Res.*, *110*, B05S06, doi:10.1029/2004JB003245.

Papazachos, B., and C. Papazachos (2000), Accelerated preshock deformation of broad regions in the Aegean area, *Pure Appl. Geophys.*, *157*, 1663–1681.

Papazachos, B. C., A. S. Savvaidis, G. F. Karakaisis, and C. B. Papazachos (2002a), Precursory accelerating seismic crustal deformation in the northwestern Anatolia fault zone, *Tectonophysics*, *347*, 217.

Papazachos, B. C., A. S. Savvaidis, C. B. Papazachos, and G. F. Karakaisis (2002b), Precursory seismic crustal deformation in the area of southern Albanides, *J. Seismol.*, *6*, 237–245.

Papazachos, C. B., G. F. Karakaisis, A. S. Savvaidis, and B. C. Papazachos (2002c), Accelerating seismic crustal deformation in the southern Aegean area, *Bull. Seismol. Soc. Am.*, *92*, 570–580, doi:10.1785/0120000223.

Pollitz, F., W. H. Bakun, and M. Nyst (2004), A physical model for strain accumulation in the San Francisco Bay region: Stress evolution since 1838, *J. Geophys. Res.*, *109*, B11408, doi:10.1029/2004JB003003.

Robinson, R. (2000), A test of the precursory accelerating moment release model on some recent New Zealand earthquakes, *Geophys. J. Int.*, *140*, 568–576.

Robinson, R., S. Zhou, S. Johnston, and D. Vere-Jones (2005), Precursory accelerating seismic moment release (AMR) in a synthetic seismicity catalog: A preliminary study, *Geophys. Res. Lett.*, *32*, L07309, doi:10.1029/2005GL022576.

Saleur, H., C. G. Sammis, and D. Sornette (1996), Discrete scale invariance, complex fractal dimensions, and log-periodic fluctuations in seismicity, *J. Geophys. Res.*, *101*, 17,661–17,677.

Sammis, C. G., and S. W. Smith (1999), Seismic cycles and the evolution of stress correlation in cellular automaton models of finite fault networks, *Pure Appl. Geophys.*, *155*, 307–334.

Sammis, C. G., D. D. Bowman, and G. C. P. King (2004), Anomalous seismicity and accelerating moment release preceding the 2001 and 2002 earthquakes in northern Baja California, Mexico, *Pure Appl. Geophys.*, *161*, 2369–2378.

Smalley, R. F., D. L. Turcotte, and S. A. Solla (1985), A renormalization group approach to the stick-slip behavior of faults, *J. Geophys. Res.*, *90*, 1894–1900.

Sornette, A., and D. Sornette (1990), Earthquake rupture as a critical point: Consequences for telluric precursors, *Tectonophysics*, *179*, 327–334.

Sornette, D., and C. G. Sammis (1995), Complex critical exponents from renormalization group theory of earthquakes: Implications for earthquake predictions, *J. Phys. I*, *5*, 607–619.

Stein, R. S. (1999), The role of stress transfer in earthquake occurrence, *Nature*, *402*, 605–609.

Stein, R. S., G. C. P. King, and J. B. Rundle (1988), The growth of geological structures by repeated earthquakes: 2. Field examples of continental dip-slip faults, *J. Geophys. Res.*, *93*, 13,319–13,331.

Sykes, L., and S. Jaumé (1990), Seismic activity on neighboring faults as a long-term precursor to large earthquakes in the San Fransisco Bay area, *Nature*, *348*, 595–599.

Tiampo, K. F., J. B. Rundle, and W. Klein (2006), Premonitory seismicity changes prior to the Parkfield and Coalinga earthquakes in southern California, *Tectonophysics*, *413*, 77–86.

Toda, S., and R. S. Stein (2000), Did stress triggering cause the large off-fault aftershocks of the 25 March 1998 M_w = 8.1 Antarctic Plate earthquake?, *Geophys. Res. Lett.*, *27*, 2301–2304.

Toda, S., and R. S. Stein (2002), Response of the San Andreas fault to the 1983 Coalinga-Nuñez earthquakes: An application of interaction-based probabilities for Parkfield, *J. Geophys. Res.*, *107*(B6), 2126, doi:10.1029/2001JB000172.

Toda, S., and R. Stein (2003), Toggling of seismicity by the 1997 Kagoshima earthquake couplet: A demonstration of time-dependent stress transfer, *J. Geophys. Res.*, *108*(B12), 2567, doi:10.1029/2003JB002527.

Utsu, T. (1961), A statistical study on the occurrence of aftershocks, *Geophys. Mag.*, *30*, 521–605.

Vere-Jones, D., R. Robinson, and W. Yang (2001), Remarks on the accelerated moment release model: Problems of model formulation, simulation and estimation, *Geophys. J. Int.*, *144*, 517–531.

Wang, W.-H., and C.-H. Chen (2001), Static stress transferred by the 1999 Chi-Chi, Taiwan, earthquake: Effects on the stability of the surrounding fault systems and aftershock triggering with a 3D fault-slip model, *Bull. Seismol. Soc. Am.*, *91*, 1041–1052.

Wiemer, S., and M. Wyss (1994), Seismic quiescence before the Landers (M = 7.5) and Big Bear (M = 6.5) 1992 earthquakes, *Bull. Seismol. Soc. Am.*, *84*, 900–916.

Zöller, G., S. Hainzl, and J. Kurths (2001), Observation of growing correlation length as an indicator for critical point behavior prior to large earthquakes, *J. Geophys. Res.*, *106*, 2167–2176.

D. D. Bowman, Department of Geological Sciences, California State University, Fullerton, CA 92834-6850, USA. (dbowman@fullerton.edu)

G. C. P. King and A. Mignan, Laboratoire Tectonique, Institut de Physique du Globe de Paris, 4, place Jussieu, F-75252 Paris Cedex 05, France.